Can homogeneous nucleation resolve the inner core nucleation paradox?

Alfred J. Wilson
School of Earth and Environment, University of Leeds
a.j.wilson1@leeds.ac.uk

Dario Alfè
Department of Earth Sciences, University College London
London Centre for Nanotechnology, Thomas Young Centre, University College London
Dipartimento di Fisica “Ettore Pancini”, Universita‘ di Napoli
d.alfe@ucl.ac.uk

Andrew M. Walker
Department of Earth Sciences, University of Oxford
andrew.walker@earth.ox.ac.uk

Christopher J. Davies
School of Earth and Environment, University of Leeds
c.davies@leeds.ac.uk

This is non-peer reviewed preprint submitted to EarthArxiv, also submitted to Earth and Planetary Science Letters for peer review.

Highlights

Can homogeneous nucleation resolve the inner core nucleation paradox?

Alfred J. Wilson, Dario Alfè, Andrew M. Walker, Christopher J. Davies

- Nucleation paradox shows inner core must be supercooled $\geq$700 K to freeze.
- Atomistic models in this study simulate Fe-rich liquids to characterise nucleation.
- Si and S both reduce nucleation rates whilst O and C increase rates.
- 3% C can reduce supercooling needed to 612 K which is close to resolving paradox.

Can homogeneous nucleation resolve the inner core nucleation paradox?

Alfred J. Wilson[a], Dario Alfè[b,c,d], Andrew M. Walker[e], Christopher J. Davies[a]

[a] *School of Earth and Environment, University of Leeds, Woodhouse, Leeds, LS2 9JT, UK*
[b] *Department of Earth Sciences, University College London, 5 Gower Place, London, WC1E 6BS, UK*
[c] *London Centre for Nanotechnology, Thomas Young Centre, University College London, 17-19 Gordon Street, London, WC1H 0AH, UK*
[d] *Dipartimento di Fisica "Ettore Pancini", Universita' di Napoli "Federico II", Monte S. Angelo, Napoli, 80126, Italy*
[e] *Department of Earth Sciences, University of Oxford, S Parks Rd, Oxford, OX1 3AN, UK*

Abstract

The formation of Earth's solid inner core is thought to mark a profound change in the evolution of the deep Earth and the power that is available to generate the geomagnetic field. Previous studies generally find that the inner core nucleated around 0.5-1 billion years ago, but neglect the fact that homogeneous liquids must be cooled far below their melting point in order for solids to form spontaneously. The classical theory of nucleation predicts that the core must be undercooled by several hundred K, which is incompatible with estimates of the core's present-day temperature. This "inner core nucleation paradox" therefore asserts that the present inner core should not have formed, leaving a significant gap in our understanding of deep Earth evolution. In this paper we explore the nucleation process in as yet untested

iron-rich systems which may comprise the Earth's early core. We find that 1 mol.% Si and S increase the supercooling required to freeze the inner core compared to pure iron by 400 K and 1000 K respectively. 3 mol.% C reduces the inner core nucleation temperature to only 612 (±139) K, which is close to resolving the paradox but still requires that the inner core formed recently.
Keywords: Inner Core, Nucleation, Molecular Dynamics

1. Introduction

The Earth's magnetic field is produced by the geodynamo in the liquid outer core. The majority of the convective power which drives the present dynamo is from inner core growth (Labrosse, 2015; Nimmo, 2015a; Davies, 2015), where light elements partitioned to the liquid create a positive buoyancy anomaly at the innermost outer core. This field shields the Earth's surface from potentially harmful space weather events and solar radiation. Palaeomagnetic records suggest that the geodynamo could have been extant for at least the last 3.4 Gyrs (Tarduno et al., 2010). Prior to inner core growth, the geodynamo must have been powered by other means such as secular cooling, radiogenic heating or precipitation of light elements (O'Rourke and Stevenson, 2016; Hirose et al., 2017; Badro et al., 2018; Wilson et al., 2022). Because it presents such a fundamental change in regimes, the nucleation of the inner core is perhaps the most important event in the thermal history of the core and might present an observable signature in the paleaomagnetic record (Biggin et al., 2015; Bono et al., 2019; Zhou et al., 2022;

Davies et al., 2022). Despite this the age of the inner core is unknown and controversy over the thermal conductivity of the core has led to a wide range of inner core age estimates (e.g. Nimmo, 2015b; Labrosse, 2015; Driscoll and Davies, 2023) from 1 Ga to 500 Ma.

Adding to the controversial timing of inner core formation, a more recent problem has come to light. Theory and atomic scale simulations predict that there is a substantial barrier to the formation of new solid in liquid iron under core conditions (Huguet et al., 2018; Davies et al., 2019; Wilson et al., 2021) that means substantial supercooling is expected to be needed before inner core formation.

Classical nucleation theory (CNT, e.g. Christian, 2002) describes the thermodynamics of nucleation and states that for a liquid to freeze it must be supercooled. This is because whilst the liquid will be thermodynamically unfavourable compared to the solid for a system below its melting temperature, the interface between the first solid and the remaining liquid comes with an energetic penalty. Only when a critical nucleus size is exceeded will the energetic preference for the solid phase outweigh the energetic penalty due to the interface. Nuclei which grow larger than this will become increasingly likely to continue to grow, leading to the system freezing. Huguet et al. (2018) used CNT to describe the supercooling needed to freeze liquid iron in the core. Applying existing calculations of interfacial energy and enthalpy of fusion of iron (Zhang et al., 2015) to define the balance of energies, the authors found that a supercooling on the order of 1000 K was needed for

spontaneous nucleation. Huguet et al. (2018) estimated the allowed supercooling by finding the largest feasible present-day separation of separation of isentrope and melting curve at the centre of the Earth whilst preserving an intersection at the inner core boundary (ICB). It is this miss-match between the predicted and allowed supercooling of the core which is the inner core nucleation paradox.

Following the discovery of the paradox, several studies have examined the problem in hopes of a resolution. Davies et al. (2019) directly observed homogeneous nucleation in molecular dynamic simulations of Fe and FeO systems at extreme supercooling and extrapolated results to Earth-like conditions, confirming the existence of the paradox. Others have probed the relevant conditions with molecular dynamic simulations of pure Fe to characterise the size distribution of sub-critical (those which re-melt) nucleation events (Wilson et al., 2021). Both approaches, find that these simple systems reproduce the original prediction of Huguet et al. (2018) with a 675 - 807 K supercooling requirement for spontaneous homogeneous nucleation of the inner core. A metadynamic approach shows that metastable iron phases may lower the nucleation barrier in a two-step nucleation process (Sun et al., 2022) but much of this reduction is owed to a lower melting temperature and this metastable phase has not been reported in molecular dynamic studies of the same systems (Davies et al., 2019; Wilson et al., 2021). A recent laser driven shock experiment study on the melting curve of iron has suggested that the paradox does not exist and that the nucleation barrier is far lower

than previously thought for planetary interiors (Kraus et al., 2022). This assertion is based on the freezing of a sample in only a few nanoseconds, far faster than predicted by CNT, but used Fe foils with impurities, which might lower interfacial energies, and an experimental configuration which provides heterogeneous nucleation sites. Both of these effects can reduce the nucleation barrier and increase nucleation rates but would not be present in the core.

All prior studies have focused almost exclusively on pure iron systems with the exception of Davies et al. (2019) who found $Fe_{0.9}O_{0.1}$ had little effect on the required supercooling due to almost equal but opposite effects of reducing the nucleation barrier and melting point depression. The composition of the core is to be expected far more complex, with an overall density deficit of $\sim$10% attributed to dissolved light elements (Anderson, 2002) and the density contrast between outer and inner core requiring compositional variation within the core (Davies et al., 2015). Silicon, sulphur, carbon and oxygen are all candidate light elements in the core (Hirose et al., 2021) due to their solubility in liquid iron at high temperature and their abundance in the mantle, although their effects on nucleation are unlikely to be similar. For example, because silicon and sulphur do not strongly partition to the solid (Alfè et al., 2002b; Alfe et al., 2000), they are expected to depress the melting curve of Fe less than carbon and oxygen, which do (Li et al., 2019; Alfè et al., 2007).

This study will examine whether iron-rich binary alloys with compositions

thought to be relevant to Earth's core are capable of spontaneous homogeneous nucleation at supercooling which would resolve the inner core nucleation paradox. We only consider homogeneous nucleation because there are no obvious solid surface on which iron can first nucleate at the centre of the core. We will first describe the methods used to simulate supercooled liquids and characterise nucleation within them following our previous work (Wilson et al., 2021). We will then present predictions of critical nucleus sizes for Fe_xO_{1-x}, Fe_xC_{1-x}, Fe_xSi_{1-x} and Fe_xS_{1-x} at $x = 1$ and 3 mol. %. Finally, we will compare the rate at which the critical events are achieved to a revised estimate of the geophysically viable supercooling in the core.

2. Methods

This study aims to define the supercooling required to freeze iron-rich systems under the conditions of Earth's core. CNT is applied to describe the thermodynamic process of supercooled liquids freezing. In order to characterise nucleation, we require models which accurately describe molecular dynamic behaviour whilst having the computationally efficiency to perform simulations of many thousands of atoms running for long periods of time and thus generate useful statistics. Embedded atom models (EAMs) are used for these simulations and first principles calculations define the parameters of these models. To frame these calculations at relevant pressure and temperatures, equations of state and melting curves must also be calculated for these models. We use the methodology of Wilson et al. (2021) expanded

to binary systems to identify nuclei, calculate nucleation rates and predict waiting times for systems to freeze.

2.1. Classical Nucleation Theory

The rate per unit volume at which nuclei spontaneously form (I) in a supercooled liquid is

$$I(r) = I_0 \exp\left(\frac{-\Delta G(r)}{k_B T}\right), \tag{1}$$

where r is the radius of the nucleus, I_0 is a prefactor scaling the kinetics of the system, ΔG is the free energy associated with forming the nucleus, k_B is the Boltzmann constant and T is temperature. As discussed earlier, ΔG is comprised of a favourable term associated with converting liquid to solid and an unfavourable term associated with forming an interface between the states. For a sphere

$$\Delta G(r) = \frac{4}{3}\pi r^3 g^{sl} + 4\pi r^2 \gamma, \tag{2}$$

where γ is the interfacial energy and g^{sl} is the difference between the free energy of the solid and the liquid ($g^{sl} = g^s - g^l$). g^{sl} can be approximated through the enthalpy of fusion, h_f and an accommodation for second order non-linearity in the temperature dependence, h_c,

$$g^{sl} = h_f \frac{\delta T}{T}\left(1 - h_c \delta T\right). \tag{3}$$

g^{sl} varies with temperature and supercooling ($\delta T = T - T_m$) whilst γ is constant to a first approximation. This means that under CNT, the scaling of g^{sl} with T is what drives the exponential relation of nucleation rate with temperature in Eq. 1. Liquids must be supercooled to freeze because no part of ΔG is favourable otherwise, furthermore, Eq. 1 shows that at the melting temperature, the nucleation rate of all nuclei is infinitesimally small.

The nucleation barrier (Eq. 2) is dominated by γ at small r because of high surface area to volume ratio. All nuclei must grow from a single atom through all smaller nuclei sizes before a system can be completely frozen. The value of ΔG increases with r to a peak at which point the probability of continued growth is equal to that of remelting. This is the critical size, r_c, beyond which, the continued growth of a nucleus becomes exponentially more likely and so will usually result in the system freezing. r_c is found by evaluating the peak of the barrier, where the gradient of ΔG with respect to radius is zero

$$\frac{\delta \Delta G}{\delta r} = 0 \tag{4}$$

gives

$$r_c = \frac{-2\gamma}{g^{sl}}. \tag{5}$$

Combining Eq. 1-3 with Eq. 5 then gives the rate at which the critical event occurs, the inverse of which is the average waiting time between critical events

$$\tau_w = \tau_0 \exp\left(\frac{\Delta G(r_c)}{k_B T}\right), \tag{6}$$

where

$$\tau_0 = \frac{z}{NS}, \tag{7}$$

and

$$z = \left(\frac{\frac{4}{3}\pi r_c^3 g^{sl}}{k_B T} \right)^{-1/2}. \tag{8}$$

Here, S, N and z are the rate of nuclei growth, number of available nucleation sites and Zeldovich factor, respectively. With this formulation, once we know the thermodynamic properties of the system we can evaluate the value of δT compatible with the available incubation time for the inner core. We use CMD simulations to observe sub-critical ($r < r_c$) nuclei and record I, the distributions of which inform the thermodynamic quantities in Eq. 2 (see section 2.4 for details).

2.2. Molecular dynamics

Simulations must contain tens of thousands of atoms and be observed for several nanoseconds in order to provide useful statistics (many orders of magnitude larger and longer than possible with first principles calculations) because larger nuclei are significantly more rare than smaller ones (Eq. 1). Embedded atom models define these large scale classical molecular dynamic simulations and are fit to first principles molecular dynamics simulations for high accuracy. First principles calculations provide trajectories, energies and pressures which are fit using embedded atom models. We follow the work of Davies et al. (2019) and Wilson et al. (2021) using existing EAM parameters for pure iron (Alfè et al., 2002a) and fitting for the additional components

(Eq.s 9-15).

EAMs define the total energy of a system (E) through the sum of energies contributed by each atom (i) from the pairwise interaction with other atoms (j)

$$E = \sum_{i=1}^{N_{Fe}} E_i^{Fe} + \sum_{i=1}^{N_X} E_i^X + \sum_{i=1}^{N_{FeX}} E_i^{FeX}. \tag{9}$$

For the binary systems considered here this consists of iron-iron, iron-solute and solute-solute interactions. Each of these energies includes a repulsive term (Q), which depends on the separation of the pair (r_{ij}), and an embedded term (F) which depends on the electron density between the pair (ρ_{ij})

$$E_i^{Fe} = Q_i^{Fe} + F^{Fe}(\rho_i^{Fe}) = \sum_{j=1, j\neq i}^{N_{Fe}} \epsilon^{Fe} \left(a^{Fe}/r_{ij}\right)^{n^{Fe}} - \epsilon^{Fe} C^{Fe} \sqrt{\rho_i^{Fe}}, \tag{10}$$

$$E_i^X = Q_i^X + F^X(\rho_i^X) = \sum_{j=1, j\neq i}^{N_X} \epsilon^X \left(a^X/r_{ij}\right)^{n^X} - \epsilon^X C^X \sqrt{\rho_i^X}, \tag{11}$$

$$E_i^{FeX} = Q_i^{FeX} = \frac{1}{2} \sum_{i=1}^{N_{Fe}} \sum_{j=1, i\neq j}^{N_X} \epsilon^{FeX} \left(a^{FeX}/r_{ij}\right)^{n^{FeX}}, \tag{12}$$

where ϵ, a, n and C are free parameters specific to each interaction. The electron densities are also defined in terms of a radial separation

$$\rho_i^{Fe} = \sum_{j=1, j\neq i}^{N_{Fe}} \left(a^{Fe}/r_{ij}\right)^{m^{Fe}} + \rho_i^{FeX}, \tag{13}$$

$$\rho_i^X = \sum_{j=1,j\neq i}^{N_x} \left(a^x/r_{ij}\right)^{m^X} + \rho_i^{FeX}, \tag{14}$$

$$\rho_i^{FeX} = \sum_{j=1,j\neq i}^{N_x} \left(a^{FeX}/r_{ij}\right)^{m^{FeX}}, \tag{15}$$

and include an additional parameter m^{Fe}, m^X and m^{FeX} for each class of interaction. Details of first principles calculations, fitting of EAMs and subsequent validation can be found in the supplementary information.

Davies et al. (2019) present a model for the FeO system which we adopt here, negating the need for fitting this system. EAMs were further validated through the mean square root of the fluctuations in energy differences between configurations evaluated through EAM potentials and independent DFT simulations (not used for the fitting procedure). For $Fe_{0.97}Si_{0.03}$, $Fe_{0.97}S_{0.03}$ and $Fe_{0.97}C_{0.03}$ at 6000 K these are 0.245, 0.325 and 0.360 eV per cell respectively, which is less than k_BT (0.517 eV).

CMD simulations were conducted using the LAMMPS package (Plimpton, 1995) within the canonical ensemble. Systems contain 21296 atoms with periodic boundary conditions and trajectories calculated via the Verlet algorithm. Uniquely random initial configurations of iron atoms interspersed with each impurity are evolved for 2 ps at 10000 K to remove any pre-existing structure in the liquid. The system is then cooled to the desired temperature over 1 ps and then evolved for 1 ns, recording atom positions every 100 steps. Volumes are adjusted for each temperature and composition ac-

cording to Birch–Murnaghan 3rd order equations of state (Birch, 1947) also calculated using the EAMs.

2.3. Melting temperatures and equations of state

Melting temperatures are necessary to evaluate Eq. 3 and frame the supercooling of a system more generally. We calculate self-consistent melting temperatures for the systems studied here through coexistence simulations. These involve simulating conditions close to a point on the melting curve with regions of both solid and liquid within a single system. When the system is allowed to evolve under the microcanonical ensemble some portion of either phase will convert to the other in order to establish an equilibrium whilst maintaining constant energy and the temperature of the system will adopt a point on the melting curve. Melting point depression for Si, C and O are presented in table 1 and Fig. 1. The value of O is taken from Davies et al. (2019) and other systems are polynomials fit to our coexistence simulation results.

2.4. Nuclei identification

The conditions of interest for nucleation the Earth's inner core involve a maximum volume of 17.62 $\times 10^{18}$ m^3 and a maximum waiting time on the order of 1 Gyrs. These are not volumes or waiting times which are accessible to molecular dynamic simulation and so the critical event cannot be observed. Instead we record sub-critical nuclei, the frequency of which is directly sampling I. Solid-like arrangements of atoms are identified within

the supercooled liquid as in our previous study (Wilson et al., 2021) which in turn uses a previously developed method for categorising local bonding environments via local order parameters (Van Duijneveldt and Frenkel, 1992; Rein ten Wolde et al., 1996; Persson et al., 2011). Nuclei are comprised of solid like atoms within bonding distance of one-another (as defined by the full width of the first peak of the radial distribution function). Nuclei sharing at least half of their atoms with another in an adjacent timestep are considered to be a time evolution of the same nuclei. This information allows the frequency and growth rate of each nuclei size to be recorded.

Following Wilson et al. (2021), we use I recorded from CMD simulations to predict r_c. By considering a single T, Eq. 1 can be expressed as

$$-\ln\left(I_T(r)\right) \propto \Delta G_T(r). \tag{16}$$

Using this approach we can interpret nucleation rates as the portion of Eq. 2 where $r < r_c$ (because the critical event will never occur within practical durations). The absolute magnitude of ΔG remains poorly constrained, meaning that g^{sl}, γ and I_0 cannot be calculated yet. Instead, we fit this distribution via

$$\Delta G_T(r) = 4/3\pi r^3 A + 4\pi r^2 B, \tag{17}$$

where A and B are variables at each T. Once fit, this distribution then predicts $r_c = -2B/A$ in the same way as Eq. 5. Once r_c is known at all temperatures, the temperature dependence of r_c is described by combining

Eq. 5 and 3 to give

$$r_c(T) = \frac{-2\gamma}{h_f \frac{\delta T}{T_m}(1 - h_c \delta T)}. \tag{18}$$

Predictions of $r_c(T)$ are fit with h_f, h_c and γ being free parameters. This leaves only τ_0 remaining to populate Eq. 6, where N and S are recorded directly from simulations and z is calculated from h_f and h_c (Eq. 7).

3. Results

CMD simulations were used to calculate melting curves, equations of state and to characterise nucleation rates. Coexistence simulations of liquid and solid were preformed at 13 volumes (corresponding to 200-400 GPa), 10 temperatures (5000-7000 K) and 4 solute concentrations (1-7 mol. %) for each system (Si, S and C). O bearing systems were only analysed for critical radius to confirm the result of Davies et al. (2019), further assessment was not warranted as this study uses the same EAM. Calculation of melting temperature (Fig. 1) is necessary due to the lack of relevant published melting curves (in terms of precise composition) and the requirement to frame sub-critical nuclei information in terms of supercooling. For the FeO system we adapt the result of Davies et al. (2019) at 323 GPa, extrapolating all points such that the pure Fe result agrees with the 6490 K value of Alfè et al. (2002b) at 360 GPa (from which the Fe EAM originates). Results in this study are evaluated at 360 GPa because the centre of the Earth will have experienced the longest incubation time for nucleating the inner core. At low solute concentration (1 mol. %) all systems see a melting point depression

of ∼50 K. At 5 mol. % concentration, FeSi and FeS systems have a similarly small $\frac{dT_m}{dx}$ whilst FeO and FeC remain approximately linear over this compositional range. This is because Si and S are partitioned equally between solid and liquid (Alfè et al., 2007), meaning the effect on free energies of solid and liquid is similar and balanced. The opposite is true of C and O, where both are more strongly partitioned to the liquid (Li et al., 2019) implying greater melting point depression. Melting point depression for O bearing systems found by Davies et al. (2019) is greater than the effect we find for systems with C.

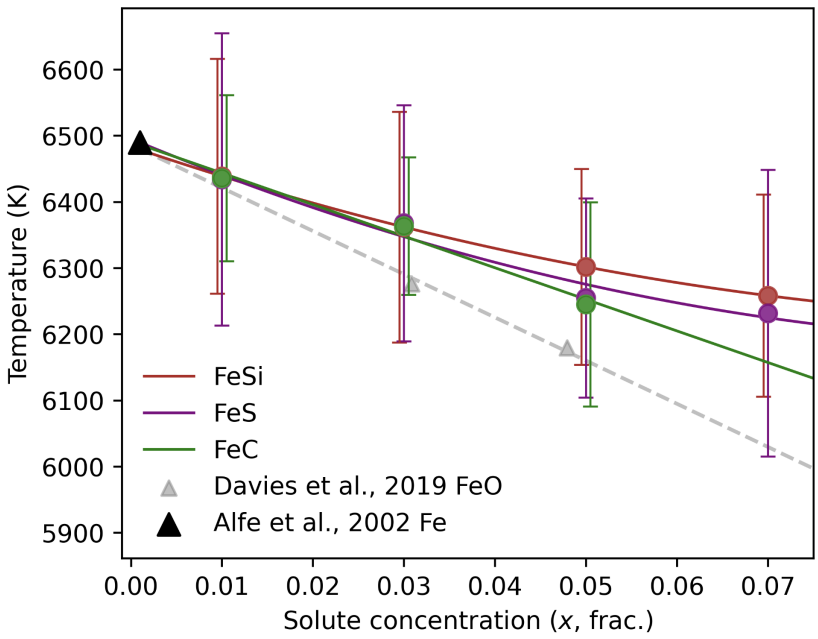

Figure 1: Melting temperatures of FeSi, FeS, and FeC (maroon, purple and green circles respectively) systems calculated via coexistence simulation at 360 GPa. All systems take a pure Fe melting temperature from Alfè et al. (2002a) (black triangle) which also provides the same Fe EAM used here. Davies et al. (2019) is shown for comparison (grey triangles and line) and is adjusted to match the pure Fe 360 GPa value.

To characterise nucleation we perform CMD calculations of supercooled systems at 5-10 temperatures and 1-3 solute concentrations in order to record the properties of sub-critical nuclei. For sufficient statistics to be gathered, we run these calculations with between 80 and 200 random initial configurations per temperature and composition, resulting in ∼6000 calculations totalling more than 50 million cpu hours.

Figure 2 shows nucleation rates in systems containing Si, S and C. Those with C have produce nuclei ∼20% faster than those containing Si and S for similar supercooling, suggesting that the nucleation barrier is lower (ΔG is smaller). It is helpful to express these results in terms of a notional radius

$$\tilde{r} = \left(\frac{N^{nuc} v_{par}}{\frac{4}{3}\pi} \right)^{1/3}, \tag{19}$$

where $v_{par} = V/N^{atoms}$, V is the volume of the system, N^{atoms} is the number of atoms in the system and N^{nuc} is the number of atoms in the nuclei. Whilst $\tilde{r}$ is framed in terms of spherical nuclei, shapes can vary from this significantly as we discuss below.

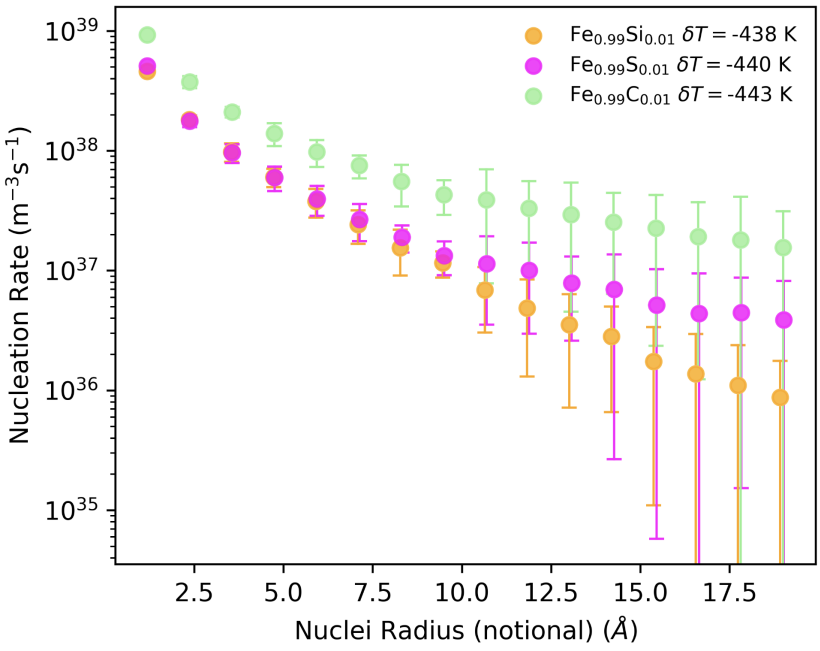

Figure 2: Nucleation rates of sub-critical nuclei for 1 mol.% Si, S and C systems (orange, magenta, light green) at similar supercooling. Size is shown as notional radius (Eq. 19). Si and S bearing systems nucleate slower than those containing O for all nuclei sizes. Whilst the functional form of these results is not important, a first order observation is that systems with C nucleate faster than others.

Simulations containing $\geq$5 mol.% solute often produced liquid regions enriched in the solute. This means that the system then contains at least two liquids, one Fe rich and another solute rich. The formulations of CNT and free energy differences applied here are not appropriate to describe these conditions. Because of this we choose not to include these concentrations here and focus on the cases where the liquid compositions remain consistently homogeneous. Despite not including these results, we observe the same phenomena of liquid phase separation in first principles calculates of smaller systems at the same conditions.

All simulations see non-spherical nuclei at small sizes (Fig. 3). CNT typically assumes a spherical geometry (e.g. Christian, 2002) despite this formulation being intended for vapour-liquid systems. Spheres are energetically preferred due to a minimisation of surface area compared to other geometries. Many solids exhibit preferred growth directions in crystal lattices where the energetic benefit of forming a non-spherical crystal can outweigh the minimised surface area of a spherical nucleus. The anisotropic nature of these situations can largely be ignored (Christian, 2002) provided that a consideration of geometry is still applied. In a previous study, we retained the spherical treatment of CNT equations, however, the distributions produced here via Eq. 16 from CMD simulations produce greater $\frac{\delta \Delta G}{\delta r}$ at small r compared to spherical geometry which is assumed by standard CNT.

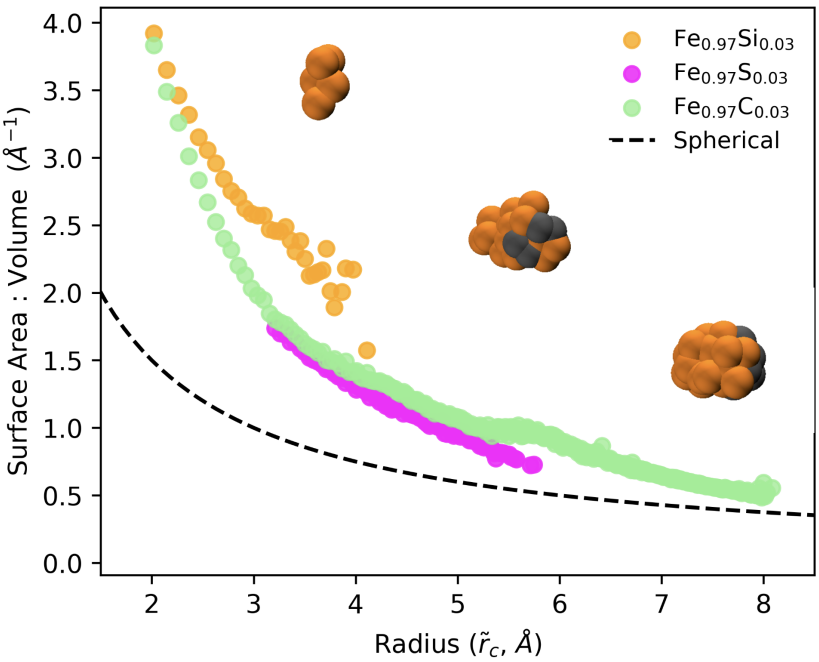

Figure 3: Surface area to volume ratio for sub-critical nuclei at ~400 K supercooling (r_c >20 Å). Systems containing 3 mol.% Si, S and C (orange, pink and green circles) are shown as well as the spherical case (black dashed line, $3r$) for comparison. Also shown are example nuclei from the C bearing system for reference. Surface area to volume ratios are similar for all systems and approach spherical before the critical size.

Whilst non-spherical small nuclei were apparent with the pure Fe system, we find the departure from sphericity to be more pronounced in impure systems. Despite this, as nuclei grow, they incorporate a greater number of defects, randomising the preferred growth direction and becoming spherical before reaching the critical size. This is true in both pure and light element bearing systems, where the pure Fe systems which freeze are best described as defect rich hexagonally close packed (hcp) structure (Wilson et al., 2021). These defects are randomly distributed and disrupt the structure of the nuclei but are able to relax from the structure to form the energetically favoured

phase given time. When nuclei first form, they contain few defects and so are most likely to have a single preferred growth in the direction of the basal plane as platelets, as is generally the case with hcp metals and alloys (Bergman et al., 2003). This is the mechanism which promotes dendritic growth in hcp structured materials and leads to small nuclei becoming elongate here.

For completeness we include a description of non-spherical geometries. The surface area to volume ratio of these geometries follows a power law decay, the same as a sphere, only with a greater initial gradient. We therefore apply Eq. 16 with $\Delta G = VA + \omega VB$ in place of Eq. 2, where V is volume of the nuclei, A and B are proxies for the free energy contributions and ω is the surface area to volume ratio $\omega = \frac{s}{V} = \alpha V^{-\beta/3}$, using α and β as fitting parameters. All results here include this modification. Despite this accommodation, the geometry of larger nuclei becomes increasingly spherical towards the critical size and the temperature dependence of r_c remains appropriately described by Eq. 18.

Through Eq. 16, nucleation rates recorded from MD simulations allow the prediction of critical radius (Fig. 4) following the methods of Wilson et al. (2021). For Si and S systems, the critical nuclei predicted are 10-100% larger than in the pure case at the same supercooling. The O bearing system matches the extrapolated result of Davies et al. (2019) where nuclei are $\sim$10% smaller than the pure Fe case for 10 mol.% O. C is more efficient at producing smaller nuclei than O. 1 mol.% C gives a similar result to 10 mol.% O for moderate supercooling, but is less efficient at small supercooling.

Extrapolation of these results to 200 K supercooling (where Huguet et al. (2018) proposed the paradox would be resolved) suggests that the small C concentrations would not reduce the barrier to nucleation compared to Fe. 3 mol.% C provides smaller critical nuclei over the 10 mol.% O case at all T studied, being ∼20% smaller than the pure Fe case.

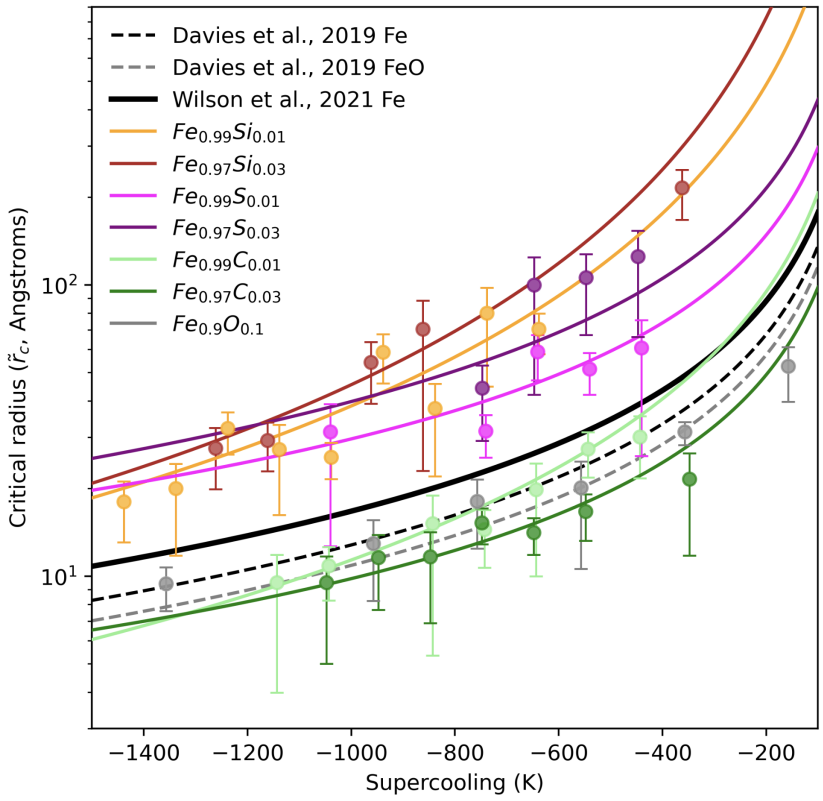

Figure 4: Critical radii sizes predicted at different δT from distributions of nuclei sizes in CMD simulations. Coloured points are the results of this study and the fits are shown as solid lines. The pure Fe results of Wilson et al. (2021) (thick black line) is shown for comparison as well as the results of Davies et al. (2019) (dashed lines). Larger critical radii than the pure Fe system are found in Si and S bearing systems, which represents a reduced nucleation rate and an increased barrier to nucleation. O and C bearing systems present increased nucleation rates relative to the pure system. Davies et al. (2019) and Wilson et al. (2021) are shown for comparison where the latter uses the same methods applied here.

Fits to the temperature dependence of r_c using Eq. 18 give the thermodynamic quantities for each system, shown in table 1. Figure 5 shows τ_0 where these parameters are used to evaluate z. The remaining components of z are the rate at which nuclei grow (S) and the number of nucleation sites present at any given time (N, unrelated to terms in EAM models). The variability across compositions and the temperatures relevant to inner core incubation is within several orders of magnitude, and far less than the variance between values applied by previous studies (Christian, 2002; Huguet et al., 2018; Davies et al., 2019). Holding τ_0 constant (as a mean of all systems and temperatures) does not greatly impact the waiting time results presented here and has been the approach of most applications of CNT previously. For completeness, we choose to include a temperature dependence in our calculation of Eq. 6. This is a linear fit to the exponent of all τ_0 ($\tau_0(T) = 10^{0.02\times\delta T+24.89}$).

	T_m K	h_f J m^{-3} $\times 10^8$	h_c	γ J m^{-2}	τ_0 s m^{-3})	ICN δT K
$Fe_{0.99}Si_{0.01}$	6439	9.8	3.1×10^{-3}	1.2	2.69×10^{22}	1230(346)
$Fe_{0.97}Si_{0.03}$	6362	3.7	9.6×10^{-3}	1.4	6.43×10^{20}	2040(233)
$Fe_{0.99}S_{0.01}$	6441	47.8	1×10^{-6}	1.1	1.64×10^{21}	1837(1125)
$Fe_{0.97}S_{0.03}$	6347	31.9	1×10^{-4}	1.1	4.29×10^{20}	2131(786)
$Fe_{0.99}C_{0.01}$	6444	57.0	1×10^{-3}	1.005	2.93×10^{23}	711(55)
$Fe_{0.97}C_{0.03}$	6348	130.0	1×10^{-6}	1.005	4.63×10^{23}	612(139)
Fe[a]	6522	7.119[1]0	6.069^{-5}	1.02	5.742×10^{44}	807
$Fe_{0.90}O_{0.10}$[b]	5987*	9.8×10^9	7.05×10^{-5}	1.02	1.26×10^{45}	730

Table 1: Thermodynamic parameters fit to $r_c(T)$ for each composition tested where all evaluations for this study were carried out at 360 GPa. τ_0 varies with temperature but is given here as the value at the temperature which coincides with the supercooling required for inner core nucleation.*Melting temperature is adjusted from the value at 323 GPa to agree with the pure Fe result of (Alfè et al., 2002a). [a]Wilson et al. (2021), [b]Davies et al. (2019)

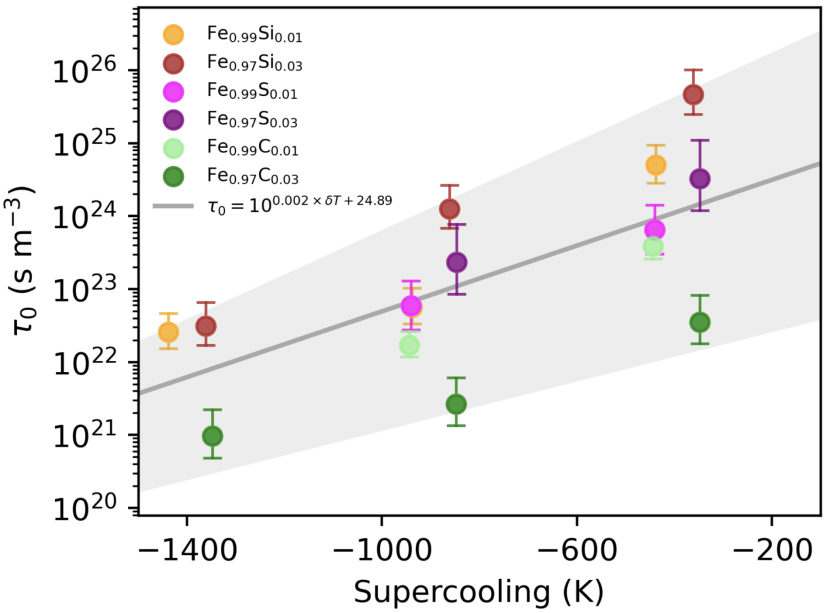

Figure 5: Prefactor to critical event waiting times calculated from values in table 1 and the growth rate (S) and number of nucleation sites (N) recorded from CMD simulations. Temperature dependence is a linear fit (grey line) of all data and the shaded region captures the uncertainty of this fit.

The difference in free energy between solid and liquid defines the energetic benefit to freezing the liquid. A more negative g^{sl} is seen for C bearing systems compared to the pure Fe system and those containing Si and S (Fig. 6). S and Si see a smaller free energy difference at all temperatures when compared to other systems (Fig. 6), agreeing with previous finding that partitioning is approximately evenly between solid and liquid iron (Alfè et al., 2007).

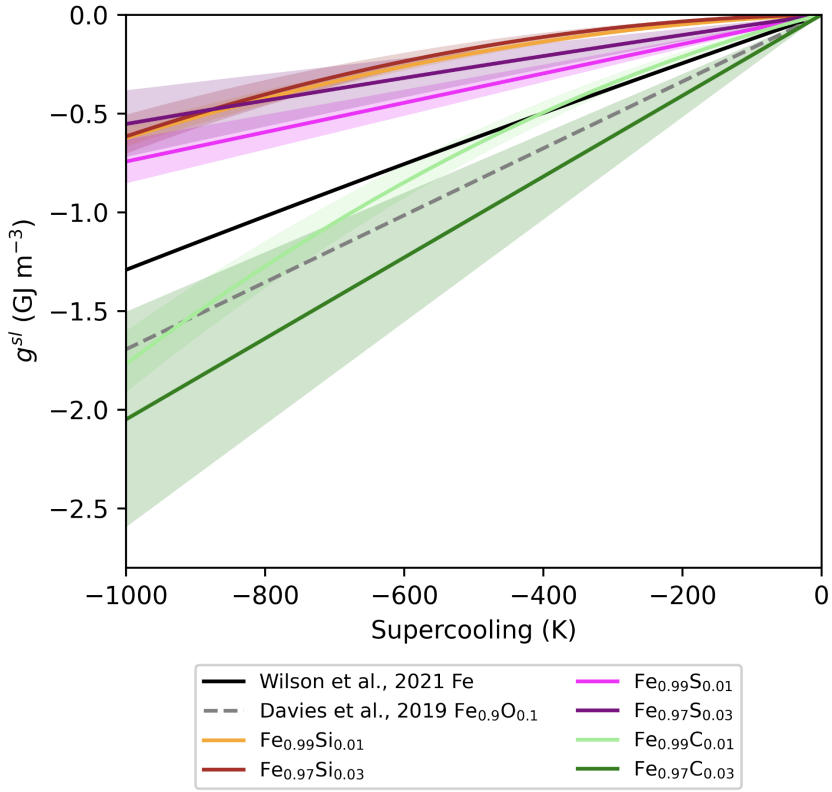

Figure 6: Comparison of $g^{sl}(T)$ from fits to $r_c(T)$ for each system studied. Dashed black line is the pure Fe case from Wilson et al. (2021) using the same methods applied here. Large differences in g^{sl} imply that the structure of nucleating material and the composition of the liquid are largely responsible for differing nucleation behaviour.

4. Discussion

Our results shown that nucleation rates in Fe rich liquids containing C are faster than those containing Si or S (Fig.2). Compared to the pure Fe system, critical nuclei sizes are larger in system containing Si and S and smaller in those containing C and O (Fig.4). These finding suggest that systems containing C and O should freeze at higher temperatures (lower supercooling) than a pure Fe system.

To asses whether the systems studied here might resolve the paradox, we must compare the time taken to nucleate at supercooling permitted in the core with the available time to nucleate in the core, the incubation time. The maximum incubation time available for the inner core to form depends on the undercooling available and the minimum age of the inner core. In the most extreme case (referred to as the extreme case hereafter) the inner core nucleated very recently and so the incubation time is the entire duration since becoming supercooled to the present day. Huguet et al. (2018) estimated a maximum allowable supercooling of $\sim$200 K by calculating separation between the isentrope and melting curve at the centre of the Earth whilst preserving the intersection of melting curve and temperature profile at the present inner core boundary. To do this, the authors defined a melting curve with Lindemann's law and the result of Anzellini et al. (2013), and an isoentrope from Labrosse (2003), both populated with material properties of the core. By varying the parameters of these functions within their uncertainty, the authors found that the maximum supercooling at the centre of

the core is ∼200 K. This would translate to a 1 Gyr maximum incubation time if the core is cooling at ∼200 K Gyr^{-1}.

We consider two cases, the extreme case and a more moderate version where the inner core is not required to have nucleated recently. For the extreme case we take a similar approach to Huguet et al. (2018) but explore a greater range of input parameters in these functions. Additionally, if the thermal conductivity of the core is both high and depth dependent then the centre of the core can become thermally stratified (Gomi et al., 2013). In this case the temperature profile of the core would not be isentropic and could be isothermal at an extreme. We vary the parameters of the adiabat and the effect of melting point depression on the melting curves of Alfè et al. (2002c); Sinmyo et al. (2019). These melting curves are chosen to explore different predicted gradients at the ICB. Figure 7 presents some of these combinations, including a case showing the maximum permissible supercooling of 419 K. This means that the extreme case incubation time for the core could be 2.4 $\times 10^{35}$ s m^3, more than double that used by previous studies. For a moderate case, which might offer a resolution to the paradox whilst being plausible to incorporate into thermal histories of the core, we take the extreme case without exploring the uncertainties or melting point depression. With an isothermal inner core the maximum permissible supercooling is ∼400 K. Most importantly, we consider that the incubation volume is half the radius of the present inner core, implying that the remaining half (87.5% of volume) of the inner core froze slowly as the core cooled. The incubation for this moderate

420 case is 1.7 $\times 10^{29}$ s m^3, and provides a sense of the time available to not just
421 resolve the paradox, but do so with the inner core age being compatible with
422 thermal history models of the core.

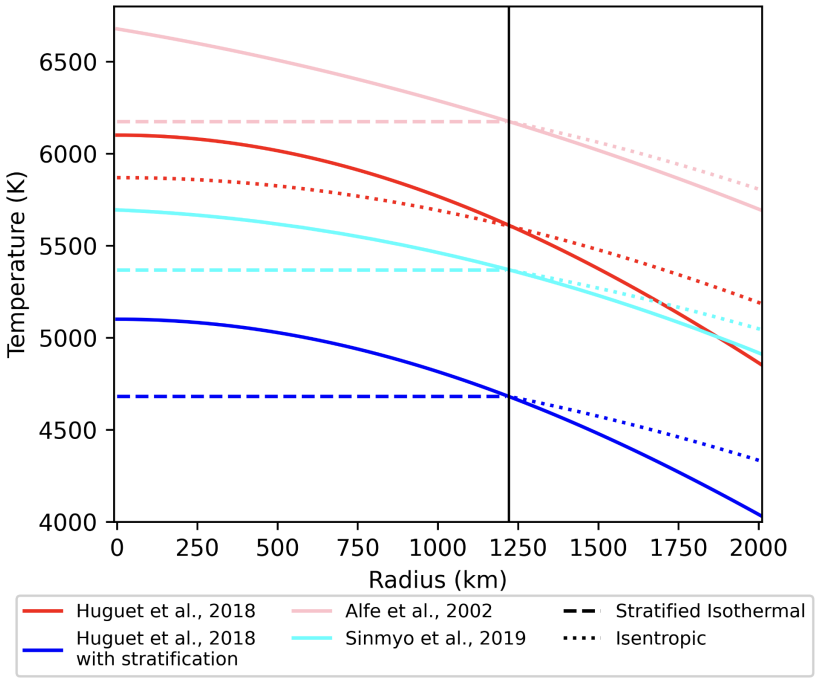

Figure 7: Melting curves (solid lines) and core temperature profiles (dotted and dashed lines) with radius. Dotted (dashed) lines represent isentropic (isothermal) regions of the core. Temperature profiles are described by varying the material properties of the core used by Huguet et al. (2018) within uncertainty and also considering thermal stratification of the innermost core. Melting curves from Huguet et al. (2018) (red, blue), Alfè et al. (2002a) (pink) and Sinmyo et al. (2019) (cyan) are also applied (with varying degrees of melting point depression, causing the apparent separation) to find the largest plausible separation of temperature and melting point, and therefore supercooling, at 360 GPa whilst preserving an intersection at the ICB (solid black line).

423 The duration before a supercooled system will producing a critical event
424 and freeze is presented here as waiting time (Fig. 8). As predicted by a lower
425 nucleation rates, larger critical nuclei and less favourable thermodynamic

properties; Si and S bearing systems require significantly greater supercooling than the pure iron system. In reality these systems would simply freeze via alternate mechanisms, the fluctuations of composition we observe in high solute concentration systems would produce Fe rich regions spontaneously. This would result in an elevated nucleation rate due to a more pure Fe system, meaning that freezing would occur at supercooling closer to that described by the pure Fe case. In the case of FeO systems, our results confirm those of Davies et al. (2019), where 730 K of supercooling is needed to nucleate the inner core.

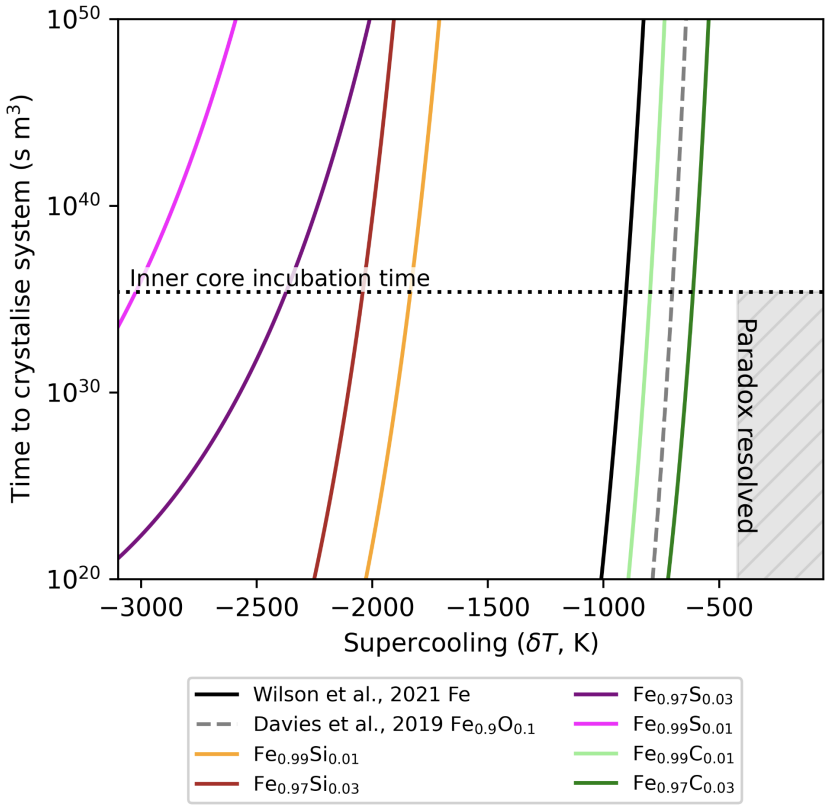

Figure 8: Average waiting time to observe freezing time against δT for different iron-rich liquids. Solid coloured lines are results of this study for systems containing Si (orange, maroon), S (pink, purple) and C (greens) where dark colours are higher solute concentration. Black (grey) line is the Fe ($Fe_{0.9}O_{0.1}$) systems from previous studies. Black dotted line represents the maximum incubation time (extreme case) available to the nucleate the inner core if the centre of the Earth is supercooled by 419 K at the present day and the core cools at 200 K Gyr^{-1}. Supercooling within the grey hatched region does not present a nucleation paradox.

Compared to all other cases considered so far, the FeC system shows a far more efficient reduction of the nucleation barrier, partly due to a smaller depression of the melting curve. 1 mol.% C requires 711 K (± 55 K) of supercooling and 3 mol.% requires cooling to 612(±139) K below melting in order to nucleate the inner core for the extreme case, close to the 419 K

of permissible supercooling of core to avoid a nucleation paradox. For the moderate case, where incubation time accounts for the core being several hundred million years old, this system requires 649($\pm$148) K of supercooling.

5. Conclusion

This study examines the effect of light elements commonly considered to be present in the core on the nucleation of the inner core. Both oxygen and carbon can make a reduction to the supercooling required to produce the first solids in the core. The best conceivable solution from the binary systems tested here is within $\sim$50 K of resolving the paradox. Other higher concentration ternary or higher order systems may surpass these results and present possible resolutions to the paradox but are beyond the capability of the methodology applied here. It should also be noted that a minimum viable resolution to the paradox still presents significant challenges for the thermal history of the core as it implies a very young inner core which is incompatible with a high thermal conductivity core and consistent geodynamo output. We find that for a more reasonable incubation time, the paradox is $\sim$30 K more difficult to resolve.

The presence of compositionally distinct regions in our simulations means a breakdown of the thermodynamic theory we apply here. If explored appropriately, these may provide alternate resolutions to the paradox; for example, through local enrichment in elements which reduce the nucleation barrier.

6. CRediT authorship contribution statement

DA produced the original embedded atom models for Fe and FeO and provided the code for fitting. AJW conducted all simulations, model fitting and validation, and analysis. AJW, CD, AMW and DA wrote the manuscript.

7. acknowledgments

We acknowledge a Natural Environment Research Council grant, reference NE/T000228/1, which supports this project. Calculations were performed on the UK National supercomputing service ARCHER2 (via allocation through the Mineral Physics Consortium).

References

Alfe, D., Gillan, M., Price, G., 2000. Constraints on the composition of the earth's core from ab initio calculations. Nature 405, 172–175.

Alfè, D., Gillan, M., Price, G., 2002a. Complementary approaches to the ab initio calculation of melting properties. The Journal of chemical physics 116, 6170–6177.

Alfè, D., Gillan, M., Price, G., 2007. Temperature and composition of the Earth's core. Contemporary Physics 48, 63–80.

Alfè, D., Gillan, M., Price, G.D., 2002b. Composition and temperature of the Earth's core constrained by combining ab initio calculations and seismic data. Earth and Planetary Science Letters 195, 91–98.

Alfè, D., Price, G., Gillan, M., 2002c. Iron under Earth's core conditions: Liquid-state thermodynamics and high-pressure melting curve from ab initio calculations. Physical Review B 65, 165118.

Anderson, D.L., 2002. The case for irreversible chemical stratification of the mantle. International Geology Review 44, 97–116.

Anzellini, S., Dewaele, A., Mezouar, M., Loubeyre, P., Morard, G., 2013. Melting of iron at earth's inner core boundary based on fast x-ray diffraction. Science 340, 464–466.

Badro, J., Aubert, J., Hirose, K., Nomura, R., Blanchard, I., Borensztajn, S., Siebert, J., 2018. Magnesium partitioning between Earth's mantle and core and its potential to drive an early exsolution geodynamo. Geophysical Research Letters 45, 13–240.

Bergman, M.I., Agrawal, S., Carter, M., Macleod-Silberstein, M., 2003. Transverse solidification textures in hexagonal close-packed alloys. Journal of crystal growth 255, 204–211.

Biggin, A.J., Piispa, E., Pesonen, L.J., Holme, R., Paterson, G., Veikkolainen, T., Tauxe, L., 2015. Palaeomagnetic field intensity variations suggest mesoproterozoic inner-core nucleation. Nature 526, 245–248.

Birch, F., 1947. Finite elastic strain of cubic crystals. Physical review 71, 809.

Bono, R.K., Tarduno, J.A., Nimmo, F., Cottrell, R.D., 2019. Young inner core inferred from ediacaran ultra-low geomagnetic field intensity. Nature Geoscience 12, 143–147.

Christian, J.W., 2002. The theory of transformations in metals and alloys. Newnes.

Davies, C., 2015. Cooling history of earth's core with high thermal conductivity. Physics of the Earth and Planetary Interiors 247, 65–79.

Davies, C., Pozzo, M., Alfè, D., 2019. Assessing the inner core nucleation paradox with atomic-scale simulations. Earth and Planetary Science Letters 507, 1–9.

Davies, C., Pozzo, M., Gubbins, D., Alfè, D., 2015. Constraints from material properties on the dynamics and evolution of Earth's core. Nature Geoscience 8, 678–685.

Davies, C.J., Bono, R.K., Meduri, D.G., Aubert, J., Greenwood, S., Biggin, A.J., 2022. Dynamo constraints on the long-term evolution of earth's magnetic field strength. Geophysical Journal International 228, 316–336.

Driscoll, P., Davies, C., 2023. The "new core paradox:" challenges and potential solutions. Journal of Geophysical Research: Solid Earth , e2022JB025355.

Gomi, H., Ohta, K., Hirose, K., Labrosse, S., Caracas, R., Verstraete, M.J., Hernlund, J.W., 2013. The high conductivity of iron and thermal evolution

of the Earth's core. Physics of the Earth and Planetary Interiors 224, 88–103.

Hirose, K., Morard, G., Sinmyo, R., Umemoto, K., Hernlund, J., Helffrich, G., Labrosse, S., 2017. Crystallization of silicon dioxide and compositional evolution of the Earth's core. Nature 543, 99–102.

Hirose, K., Wood, B., Vočadlo, L., 2021. Light elements in the earth's core. Nature Reviews Earth & Environment 2, 645–658.

Huguet, L., Van Orman, J.A., Hauck II, S.A., Willard, M.A., 2018. Earth's inner core nucleation paradox. Earth and Planetary Science Letters 487, 9–20.

Kraus, R.G., Hemley, R.J., Ali, S.J., Belof, J.L., Benedict, L.X., Bernier, J., Braun, D., Cohen, R., Collins, G.W., Coppari, F., et al., 2022. Measuring the melting curve of iron at super-earth core conditions. Science 375, 202–205.

Labrosse, S., 2003. Thermal and magnetic evolution of the earth's core. Physics of the Earth and Planetary Interiors 140, 127–143.

Labrosse, S., 2015. Thermal evolution of the core with a high thermal conductivity. Physics of the Earth and Planetary Interiors 247, 36–55.

Li, Y., Vočadlo, L., Alfè, D., Brodholt, J., 2019. Carbon partitioning between the Earth's inner and outer core. Journal of Geophysical Research: Solid Earth 124, 12812–12824.

Nimmo, F., 2015a. Energetics of the core, in: Schubert, G. (Ed.), Treatise on geophysics 2nd Edn. Elsevier, Amsterdam. volume 8, p. 27–55.

Nimmo, F., 2015b. Thermal and compositional evolution of the core. Treatise on Geophysics 9, 201–219.

O'Rourke, J.G., Stevenson, D.J., 2016. Powering Earth's dynamo with magnesium precipitation from the core. Nature 529, 387–389.

Persson, J., Desgranges, C., Delhommelle, J., 2011. Polymorph selection during the crystallization of iron under the conditions of Earth's inner core. Chemical Physics Letters 511, 57–61.

Plimpton, S., 1995. Fast parallel algorithms for short-range molecular dynamics. Journal of computational physics 117, 1–19.

Sinmyo, R., Hirose, K., Ohishi, Y., 2019. Melting curve of iron to 290 gpa determined in a resistance-heated diamond-anvil cell. Earth and Planetary Science Letters 510, 45–52.

Sun, Y., Zhang, F., Mendelev, M.I., Wentzcovitch, R.M., Ho, K.M., 2022. Two-step nucleation of the earth's inner core. Proceedings of the National Academy of Sciences 119, e2113059119.

Tarduno, J.A., Cottrell, R.D., Watkeys, M.K., Hofmann, A., Doubrovine, P.V., Mamajek, E.E., Liu, D., Sibeck, D.G., Neukirch, L.P., Usui, Y., 2010. Geodynamo, solar wind, and magnetopause 3.4 to 3.45 billion years ago. science 327, 1238–1240.

Van Duijneveldt, J., Frenkel, D., 1992. Computer simulation study of free energy barriers in crystal nucleation. The Journal of chemical physics 96, 4655–4668.

Wilson, A.J., Pozzo, M., Alfè, D., Walker, A.M., Greenwood, S., Pommier, A., Davies, C.J., 2022. Powering earth's ancient dynamo with silicon precipitation. Geophysical Research Letters 49, e2022GL100692.

Wilson, A.J., Walker, A.M., Alfè, D., Davies, C.J., 2021. Probing the nucleation of iron in earth's core using molecular dynamics simulations of supercooled liquids. Physical Review B 103, 214113.

Rein ten Wolde, P., Ruiz-Montero, M.J., Frenkel, D., 1996. Numerical calculation of the rate of crystal nucleation in a lennard-jones system at moderate undercooling. The Journal of chemical physics 104, 9932–9947.

Zhang, W.J., Liu, Z.Y., Liu, Z.L., Cai, L.C., 2015. Melting curves and entropy of melting of iron under Earth's core conditions. Physics of the Earth and Planetary Interiors 244, 69–77.

Zhou, T., Tarduno, J.A., Nimmo, F., Cottrell, R.D., Bono, R.K., Ibanez-Mejia, M., Huang, W., Hamilton, M., Kodama, K., Smirnov, A.V., et al., 2022. Early cambrian renewal of the geodynamo and the origin of inner core structure. Nature communications 13, 1–7.